Effect of stresses on the dielectric and piezoelectric properties of Pb(Zr$_{0.52}$Ti$_{0.48}$)O$_3$ thin films (EP)

K. Coleman, J. Walker, T. Beechem, and (iD) S. Trolier-McKinstry

COLLECTIONS

(EP) This paper was selected as an Editor's Pick

View Online   Export Citation   CrossMark

ARTICLES YOU MAY BE INTERESTED IN

BaTiO$_3$-based piezoelectrics: Fundamentals, current status, and perspectives
Applied Physics Reviews **4**, 041305 (2017); https://doi.org/10.1063/1.4990046

Dead layer thickness estimation at the ferroelectric film-metal interface in PZT
Applied Physics Letters **114**, 132902 (2019); https://doi.org/10.1063/1.5084019

Ferroelectric thin films: Review of materials, properties, and applications
Journal of Applied Physics **100**, 051606 (2006); https://doi.org/10.1063/1.2336999

Effect of stresses on the dielectric and piezoelectric properties of Pb(Zr$_{0.52}$Ti$_{0.48}$)O$_3$ thin films (EP)

View Online   Export Citation   CrossMark

K. Coleman,[1,a)] J. Walker,[1,2] T. Beechem,[3] and S. Trolier-McKinstry[1] (iD)

AFFILIATIONS

[1]Materials Science and Engineering Department and Materials Research Institute, Pennsylvania State University,
Millennium Science Complex, University Park, Pennsylvania 16802, USA
[2]Department of Materials Science and Engineering, Norwegian University of Science and Technology, N-7491 Trondheim, Norway
[3]Sandia National Laboratories, Albuquerque, New Mexico 87185, USA

[a)]kpc8@psu.edu

ABSTRACT

Flexible piezoelectric microelectromechanical systems can experience a wide range of stress conditions. In order to explore the functional properties over this range, the dielectric and piezoelectric properties of 0.6 μm thick {001} sol-gel Pb$_{0.99}\square_{0.01}$(Zr$_{0.52}$Ti$_{0.48}$)$_{0.98}$Nb$_{0.02}$O$_3$ (PZT) films on Si substrates and thin Ni foils were measured as a function of stress arising from thermal expansion mismatch during fabrication or applied by bending of a cantilever. Due to the differences in residual thermal stress, the remanent polarization, P$_r$, was approximately $21 \pm 0.2\,\mu$C/cm^2 and $39.5 \pm 2.3\,\mu$C/cm^2 for PZT films on Si and Ni, respectively, with the higher P$_r$ on Ni originating from more "c" domains (out-of-plane polarization) due to the compressive stresses. The link between stress and domain orientation was further explored by bending films on Ni around mandrels with known radii of curvature to apply uniaxial strains of −0.2% to 0.5%. Films on Si were only exposed to strains between −0.06% and 0.06%, because of substrate failure. For films on 50 μm thick Ni foil, under a 0.5% tensile strain, the P$_r$ decreased by 7%–10% and the permittivity increased up to 23% relative to zero applied stress samples. This trend reversed upon compressive strain. In addition, the piezoelectric coefficient, $e_{31,f}$ is reported to be $-9.0 \pm 0.45\,\mu$C/cm^2 and $-7.1 \pm 0.35\,\mu$C/cm^2 on Ni and Si, respectively, and increased in magnitude with applied uniaxial compressive strain. These changes are consistent with substantial levels of ferroelastic reorientation.

INTRODUCTION

Piezoelectric microelectromechanical systems (PiezoMEMS) based on piezoelectric thin films are used in sensors, actuators, and energy harvesting devices.[1,2] In all cases, the performance of these devices is dependent on the magnitude of the input signal (i.e., strain, voltage bias) and piezoelectric response of the film. Nb doped lead zirconate titanate [Pb$_{0.99}\square_{0.01}$(Zr$_{0.52}$Ti$_{0.48}$)$_{0.98}$Nb$_{0.02}$O$_3$, PZT] has a large piezoelectric response and is a well-established commercial piezoelectric ceramic,[1–4] prompting interest in PZT films. The morphotropic phase boundary (MPB) is of particular interest because the piezoelectric properties peak at this composition. PZT films are also commonly doped with Nb, which creates Pb vacancies (denoted as $\square$) for charge balance. Nb doping enhances domain wall mobility and increases the dielectric and piezoelectric responses. While PZT films tend to exhibit lower piezoelectric coefficients compared to their bulk counterparts, because of clamping of the film to the substrates and pinning of non-180° domain walls,[5–7] the response can be partially recovered through the use of oriented films. In addition, the achievable piezoelectric responses significantly exceed those of alternatives such as Zn$_{1−x}$Mg$_x$O and Al$_{1−x}$Sc$_x$N, making PZT films useful particularly in cases where large field-induced strains are required.[8–12]

Besides orientation, the stress state can influence the piezoelectric response of ferroelectric films like PZT.[13–15] In particular, residual stresses influence the domain structure, and as a consequence of limitations on ferroelastic domain switching, the remanent and saturation polarizations depend on the residual stresses.[16–19] Furthermore, applied stresses also affect dielectric and piezoelectric properties of all piezoelectric ceramics, although the changes tend to be smaller in magnitude for thin films than those of bulk ceramics exposed to the same stress levels.[4,5,8,20,21] For flexible devices, the

applied stresses may greatly exceed those typically found in applications utilizing "bulk" ceramics. Thus, it is necessary to explore how the piezoelectric response of thin films is altered by the combination of large residual and applied loads.

While much of the previous work concentrates on films on rigid substrates, some applications (e.g., energy harvesting devices) require flexible substrates to reach higher stress and achieve greater power densities.[9,22,23] While there are some studies on residual stresses in PZT film grown on metallic substrates,[22,24] the combination of residual and applied stresses has not been reported over wide stress ranges. Therefore, this study aims to quantify the effects of the total stress state on the piezoelectric, ferroelectric, and dielectric response of PZT thin films over these stress ranges.

The total stress (σ_{Tot}) experienced by the films includes the residual stress (σ_r), the applied stress induced by bending (σ_a), and the electric field-induced stress (σ_e) dependent on the magnitude of an applied electric field and piezoelectric coefficient, $e_{31,f}$[8] as shown in Eq. (1). In this study, only in-plane residual and applied stresses were considered. This, in turn, provides a means to monitor the magnitude of $e_{31,f}$ along with accompanying dielectric and piezoelectric properties as a function of stress,

$$\sigma_{Tot} = \sigma_r + \sigma_e + \sigma_a. \tag{1}$$

The residual stress will depend on several factors; some of these depend on the growth method used. This may include epitaxial stresses or bombardment stress. For oriented films grown through chemical solution deposition (CSD), these types of growth stresses are not present. Instead, the film's residual stress is a function of the microstructure, porosity, and the mismatch in thermal expansion of the film and the substrate.[17] In chemical solution deposition (CSD), the removal of solvents and densification during pyrolysis strongly influence the residual porosity. Porosity, in turn, reduces the film's elastic moduli, thereby modifying the resulting residual stress in the film.[21,25] The residual stress for sol-gel films can be estimated as a function of the difference in the coefficient of thermal expansion (CTE, α_{CTE}) of the film and the substrate,[16–18] modified by partial relaxation of these stresses due to either the orientation of ferroelectric domains or the curvature of the film/substrate system. The in-plane biaxial residual stress of the film can be approximated by Eq. (2), which considers the curvature of the substrate,

$$\sigma_t = \frac{\int_{T_c}^{T_{max}} (\alpha_{CTE,film} - \alpha_{CTE,substrate}) dT}{\left\{ \frac{1 - v_f}{Y_f} + \left(\frac{1 - v_s}{Y_s} \right) \left(4 \frac{t_f}{t_s} \right) \right\}}. \tag{2}$$

However, if the substrate is rigid and the film's thickness is significantly smaller than the substrate, such as the PZT on the Si case, Eq. (2) can be simplified to the common form of Eq. (3),

$$\sigma_t = \frac{Y_f}{v_f - 1} \int_{T_o}^{T_{max}} (\alpha_{CTE,film} - \alpha_{CTE,substrate}) dT, \tag{3}$$

where v is Poisson's ratio of the film (f) or the substrate (s), Y is Young's modulus (90 GPa for {001} PZT),[26] α_{CTE} is the thermal expansion coefficient, T_{max} is the crystallization temperature, and T_o is the operating temperature. Below the Curie temperature (T_c), the nucleation of ferroelectric domains with specific orientations

reduces the stress arising from the CTE mismatch.[16] In addition to estimating the residual stresses through Eqs. (2) and (3), the residual stress can be estimated by measuring the wafer curvature for rigid substrates (but not thin metallic foils). Stoney's equation for a ⟨001⟩ Si wafer[27–31] is given in Eq. (4) as

$$\sigma_f = \frac{h^2}{6t_f(S_{11}^{Si} + S_{12}^{Si})R}, \tag{4}$$

where σ_f is the film stress, t_f is the film thickness, h is the substrate thickness, $S_{11}^{Si} + S_{12}^{Si}$ are components of the elastic compliance tensor of the Si, and R is the radius of curvature (ROC).[27] Stoney's formula is not valid for the PZT on Ni foil owing to the foil's lack of rigidity. Both σ_f and σ_t do not consider the alleviation of some stress from the domain structure and can only be used as estimates for σ_r. In this work, we have employed a polycrystalline average for the thermal expansion coefficient to approximate the residual stress and use this to estimate which domain states are most likely.

Applied stresses can also induce some ferroelastic domain switching in PZT films,[20,32] and in many applications such as energy harvesters, uniaxial stresses are applied by bending a cantilever.[9,23] In this study, uniaxial strains were applied by the radius of curvature (ROC) method in which a film is wrapped around a mandrel to induce a predetermined applied strain ($\varepsilon = \delta/R$) on the film, based on the distance of the film to the neutral axis (δ). Using this method on flexible Ni foil samples allowed for a large strain range (0.5% to −0.32%), beyond which failure of the PZT/Ni stack would occur.

In this work, {001} oriented PZT [$Pb_{0.99}\square_{0.01}$ $(Zr_{0.52}Ti_{0.48})_{0.98}Nb_{0.02}O_3$] films on Ni and Si substrates were fabricated through sol-gel to investigate the influence of substrates with different thermal and mechanical properties on the properties of PZT films. A combination of electrical characterization was used to explore changes in the properties and domain structure as a function of σ_{Tot}. The permittivity and piezoelectric coefficient were measured as a function of the total stress to interrogate the relationship between stress, domain state, and stress limits of piezoelectric thin films.[4,8,16,33,34] The Rayleigh analysis was used to understand the changes in the intrinsic and extrinsic contributions to the permittivity as a function of applied strain. The sum of the intrinsic contributions (averaged domain response) and reversible domain wall motion contributions are described by the Rayleigh parameter ε_{init}.[35,36] The irreversible domain wall contributions to the dielectric permittivity are described by the α_{Ray} parameter [Eq. (5)].[35,36] The Rayleigh parameters depend on the domain structure and the ability of the domain walls to move through a potential energy landscape. These both depend on the stress state and AC electric field (E_{ac}),

$$\varepsilon_r = \varepsilon_{init} + \alpha_{Ray}E_{ac}. \tag{5}$$

This probes the underlying mechanism that governs the extent of property changes (i.e., dielectric, ferroelectric, and piezoelectric) as a function of both the applied and total stress states.

EXPERIMENTAL PROCEDURE

PZT films were grown by chemical solution deposition (CSD) on either a 50 μm thick Ni foil or 500 μm thick Si ⟨001⟩ wafers. An

Ni foil of 99.98% purity was used from Sigma Aldrich.[22] The preparation of the Ni foil to reduce NiO formation is presented in the supplementary material and follows processes reported elsewhere.[22,37] To achieve the desired {001} orientation, a LaNiO₃ (LNO) bottom electrode was deposited by CSD using an acetic acid-based solution on both the prepared Ni foil substrates and Si wafers with a 1 μm thermal oxide (NOVA Electronic Materials). Then, PZT was deposited on the bottom electrode using CSD with a 0.4M 2-methoxyethanol based solution.[38] All PZT films have a preferred {100} orientation. Details on the processing parameters are presented in the supplementary material.

The orientation and phase purity of the films were characterized by a combination of X-ray diffraction (XRD) using a PANalytical Empyrean diffractometer with a Cu K$_\alpha$ X-ray source and by a Leo 1530 Field-Emission Scanning Electron Microscope (FESEM). Lateral grain sizes were determined using the average intercept method with a minimum of six lines in varying directions and length. DC magnetron sputtered Pt top electrodes were patterned by photolithography to have diameters of 1 mm, 0.6 mm, and 0.4 mm. These samples were then cut into cantilever beams with an aspect ratio of 1:4.

The permittivity and the polarization-electric field hysteresis (P-E) loops were measured using a Hewlett Packard LCR meter and a Radiant Multiferroic test analyzer, respectively, where the applied electric field was out of plane, perpendicular to the in-plane applied and residual stresses. The P-E loops were measured using a single triangular wave form with no prepulse and a frequency of 100 Hz.

Two different methods were used to apply uniaxial stresses for the two different substrates due to their different mechanical properties and strain limitations. For the samples on Ni, the radius of curvature (ROC) method was used, where the foil was bent around a mandrel of a known radius and the distance of the film to the neutral axis was calculated to determine the applied strain and stress. The applied strain calculated was experimentally confirmed through strain gauges within 0.02% strain. To apply compressive stress, the Ni foil was curved around the inner radius of a hollow mandrel with the PZT film facing inward, and for tensile stress, the Ni foil was curved around the outer radius with the PZT film facing outward. Compressive strains of up to −0.3% were applied, as were tensile strains up to 0.47%. Above −0.3% compressive strain, delamination between layers was observed, and above 0.5% tensile strain, cracking was observed in the PZT. For the samples on Si substrates, stress was applied by a beam bending method, where a fixed free beam of the sample had an applied force at the end of the cantilever. Since the Si substrate is brittle, the range used in this study was from 0.06% compressive strain to 0.06% tensile strain. This strain range is roughly an order of magnitude smaller compared with films on Ni foils. Schematics of these uniaxial stress configurations are found in the supplementary material.

The effective transverse piezoelectric coefficient ($e_{31,f}$) was measured by poling individual electrodes on the film at 250 kV/cm, 150° C for 15 min and waiting a minimum of 12 h to allow the domain state to stabilize. The $e_{31,f}$ was measured by clamping the film at one end and actuating it with a sinusoidal strain at the opposite end, using a piezoelectric actuator stack.[33] To measure the $e_{31,f}$ as a function of stress, the samples were strained using the

beam bending method. The stack actuator was raised and lowered to change the static strain applied to the cantilevers via bending. Raising the height of the actuator puts the PZT film into more compression. Samples were flipped upside down to put the film in tension when raising the actuator. A schematic and description of this setup are found in the supplementary material.

RESULTS

The XRD pattern and FESEM images for the PZT films on Si [Figs. 1(a), 1(c), and 1(e)] and Ni foils [Figs. 1(b), 1(d), and 1(f)] are shown in Fig. 1. The grains were columnar and the average lateral grain size for these films was 80.6 ± 13.1 and 65 ± 3.5 nm for the sample on Si and Ni foils, respectively.

The PZT residual stress was estimated from σ$_t$ calculated using Eqs. (2) and (3). The thermal expansion coefficients of Si and Ni have been reported as 2.3–4.5 × 10⁻⁶/K,[39] and 13.3–17.1 × 10⁻⁶/K[40] (in the temperature range from 25 to 700 °C), respectively. For PZT, the thermal expansion coefficient is dependent on temperature and ranges from 8 × 10⁻⁶/K down to 0/K in the paraelectric phase and between 0 and 2 × 10⁻⁶/K in the ferroelectric phase, with a discontinuity at T$_c$.[16,41] The T$_c$ for these PZT samples was 336 ± 8 °C for samples on Si and 325 ± 6 °C for samples on Ni. Using Eq. (2), the PZT films on Ni foil were under a compressive stress of approximately 530 ± 30 MPa, and PZT films on Si were under a tensile stress of approximately 130 ± 30 MPa. Eq. (3) overestimates the compressive stress of the PZT on Ni but accurately reports the tensile stress (σ$_t$) for PZT on rigid Si substrates as 130 ± 30 MPa. σ$_t$ is in agreement with σ$_f$, which was confirmed through wafer curvature measurements, as described in the supplementary material.[17] Since σ$_f$ and σ$_t$ do not consider the formation of domains, which will alleviate stress, they will somewhat overestimate the magnitude of σ$_r$. However, since the film is clamped to the substrate, there is still a significant amount of residual stress.

Recognizing the difference in the residual stress, Fig. 2 compares the P-E loops of PZT on Ni and Si at 100 Hz. At the same electrical field of 900 kV/cm, P$_r$ was 21 ± 0.2 μC/cm² on Si and 39.5 ± 2.3 μC/cm² on Ni. This discrepancy is consistent with prior reports for films under tensile stress having more in-plane polarization and lower remanent polarizations.[16,22] It is notable that the PZT film on Si could be driven to a higher electric field (1400 kV/cm) and the P$_r$ improved to 26.0 ± 0.2 μC/cm². This increase was not observed for the Ni foil samples. At lower electrical fields (400 kV/cm), the P$_r$ drops to 13.2 ± 0.12 μC/cm² and 32 ± 1.6 μC/cm² for PZT films on Si and Ni, respectively. At a driving signal of V$_{ac}$ = 30 mV and 1 kHz, the permittivity was 1040 ± 20 and 600 ± 80 for the virgin films on Si and Ni foils, respectively, with loss tangents of less than 5.0% for all of the films, which also suggests differences in the percentage of in-plane polarization, where the PZT on Si would have more in-plane polarization.

In addition, Fig. 3 shows the changes in the P-E loop and P$_r$ for PZT films on Si and Ni foils at different applied strain levels. The P-E loops of films on both Si [Fig. 3(Ia)] and Ni foils [Fig. 3(IIa)] experienced a clockwise rotation under tension and a counterclockwise rotation under compression, as has been reported previously.[7] For the films on Si, P$_r$ varied from 11.7 ± 0.16 μC/cm² at 0.06%
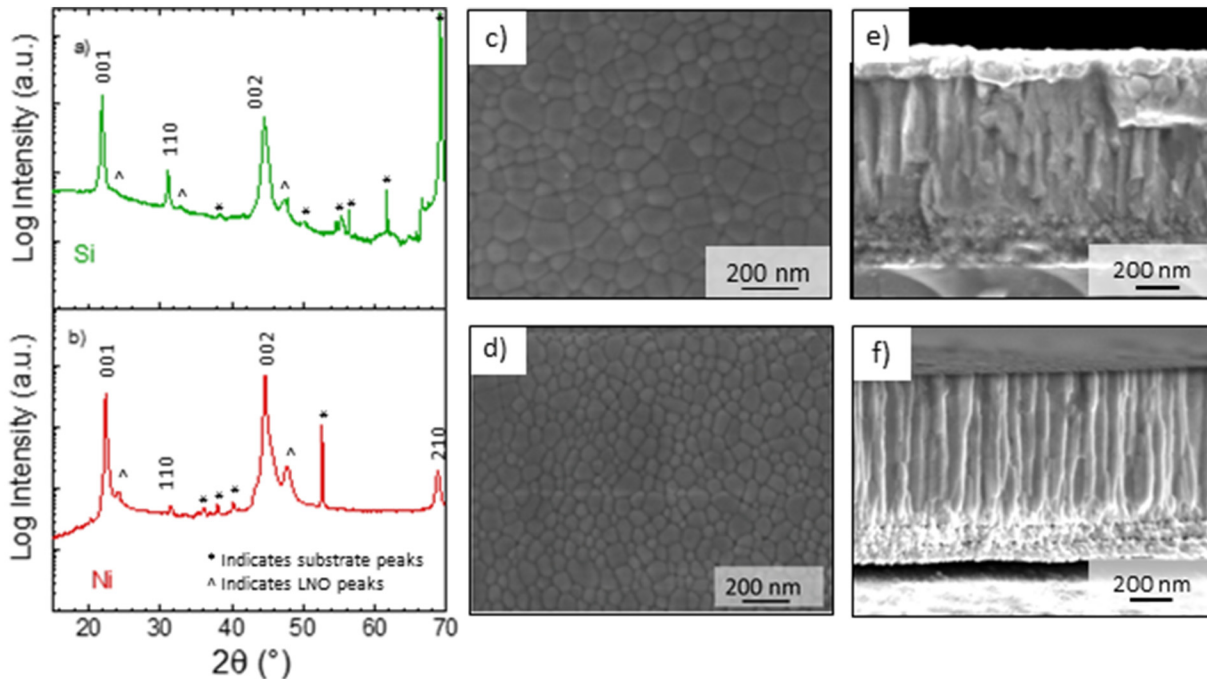
FIG. 1. XRD patterns for 0.6 μm thick PZT films on (a) Si and (b) Ni, top surface FESEM images of the grain structures on (c) Si and (d) Ni, and FESEM cross section for the 500 μm thick Si wafer (e) and 50 μm thick Ni foil (f). The Lotgering factors were 98% for the sample on the Ni foil and 92% for the sample on Si.
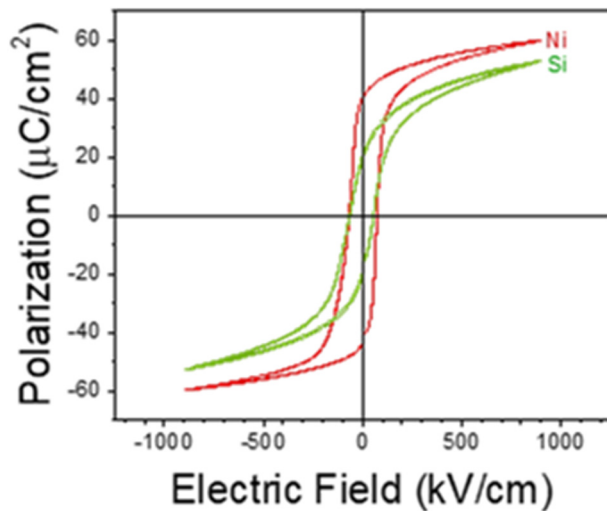
FIG. 2. The P_r for films on Si was approximately 21 μC/cm^2, while films on Ni had a P_r of 41 μC/cm^2. This was due to the compressive thermal expansion stresses for PZT films on Ni, causing a higher amount of c (out-of-plane) domain orientation.[16]

strain to 14.1 ± 0.14 μC/cm^2 at −0.06% strain at 400 kV/cm. For the films on Ni foils, P_r varied from 33 ± 1 μC/cm^2 at −0.2% strain to 27.1 ± 0.7 μC/cm^2 at 0.4% strain. Upon removing the applied strains from each sample, P_r partially recovered to the initial value at zero applied strain. These same samples were cycled through the entire strain range again; little hysteresis of P_r was observed between the first and second strain cycles for films on Si [Fig. 3(Ib)]. The hysteresis was more pronounced for PZT films on Ni substrates. However, it was still <6%, and a trend as a function of cycles was not distinguishable [Fig. 3(IIb)]. The normalized polarization changed approximately linearly as a function of applied strain for both films on Si [Fig. 3(Ic)] and Ni foils [Fig. 3(IIc)]. At 0.04% compressive strain, P_r increased by roughly 5% for the PZT on Si, while on Ni, a large compressive strain of 0.2% was required for this magnitude of a change. This difference in the strain required for a 5% change in P_r may be due to differences in the domain structure and residual stress.

To investigate how the applied strain alone influenced the domain state, dielectric Rayleigh measurements were made at 1 kHz as a function of applied strain (Fig. 4). The PZT on Ni samples were strained from −0.2% to 0.5% strain, and at 1 kHz and 0 V DC bias, the AC field was increased up to 20 kV/cm, which is less than half the coercive field. For all AC fields, the permittivity increased under applied tensile strain and decreased under compressive applied strain. At an AC driving field of 5 kV/cm (30 mV),
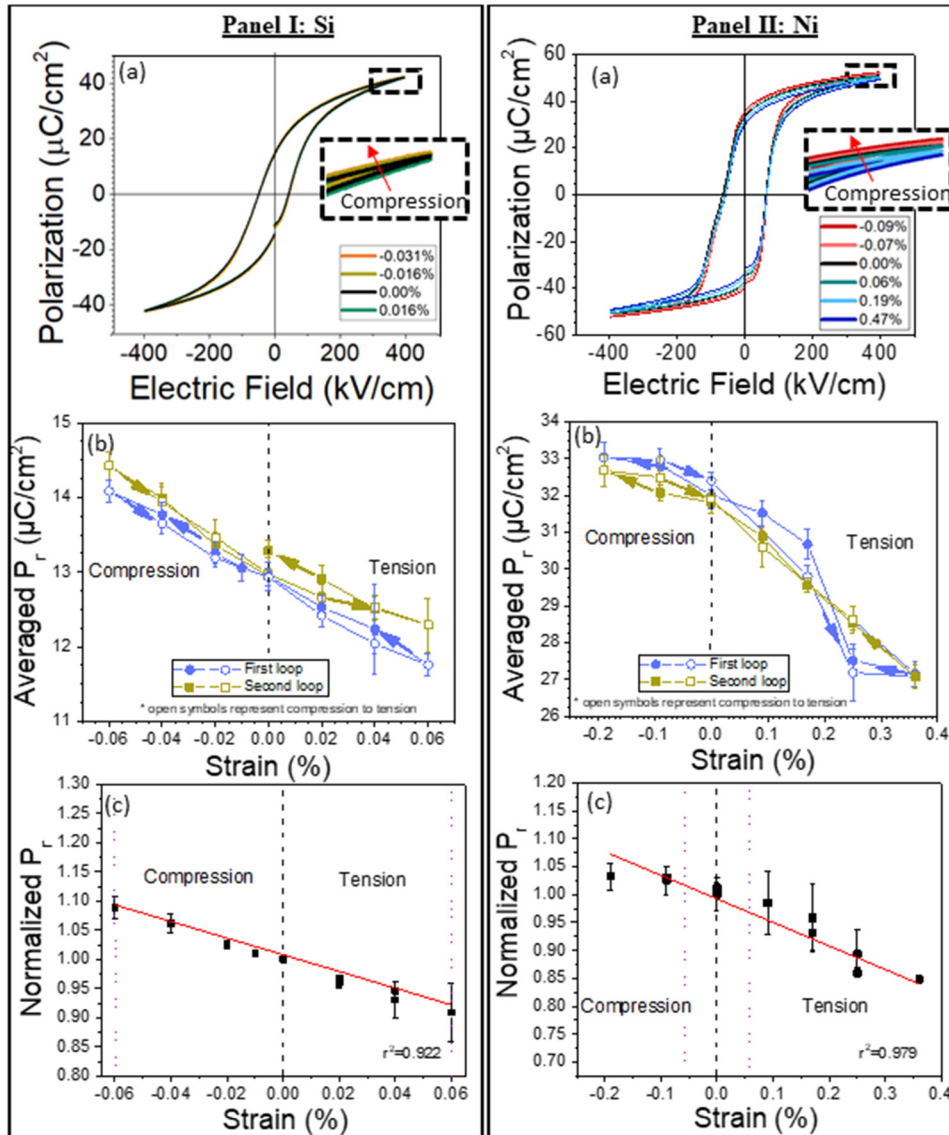
FIG. 3. Polarization hysteresis loops for PZT films on Si (Panel Ia) and Ni (Panel IIa). Changes in P_r as a function of applied compressive and tensile strain on Si (Panel Ib) and Ni (Panel IIb) as well as the linear trend of the normalized change in P_r [e.g., P_r (strain)/P_r (zero strain)] as a function of both applied compressive and tensile strain on Si (Panel Ic) and Ni (Panel IIc). The strain range for samples on Ni was −0.2% to 0.4% strain; for Si, it was from −0.06% to 0.06%. The purple dashed lines (Panel Ic and Panel IIc) indicate the smaller strain range over which films on Si were tested. Negative strains in c represent in-plane compressive strains, and positive represent in-plane tensile strain.

the permittivity for a PZT film on Ni was 620 ± 40 at 0.5% applied tensile strain and 460 ± 50 at 0.2% compressive strain [Fig. 4(b)]. The permittivity normalized to the value at zero applied strain and increased approximately linearly with the applied strain [Fig. 4(b)]. The slope of the normalized permittivity change was opposite to that of P_r. These changes are consistent with changes in the domain state under high stress levels. That is, a higher "c" domain population induced under compression should decrease the permittivity value, while a higher "a" domain population in films under tensile stress is expected to increase the permittivity.[34,42]

The permittivity in the Rayleigh regime was fitted (with an R^2 of greater than 0.999) for all strains tested and is denoted by the dashed lines in Fig. 4(a). ε_{init} is determined from the zero-field intercept, and α_{Ray} from the slope of the line. Both ε_{init} and α_{Ray}

increase with the applied tensile stress. The increase in ε_{init} may be due to an increase in reversible domain wall contributions, a change in the intrinsic response (i.e., the percentage of a increases with tension), or a combination of the two. Comparable trends in the permittivity as a function of applied strain were observed for films on Si; however, the small strain range meant that the changes in permittivity were not as pronounced as the changes observed for the P-E loops for the films on Si.

The linear increase in the low field permittivity (Fig. 4) and the linear decrease in the P_r (Fig. 3) as a function of applied tensile strain are large and suggest that tensile strain induces more in-plane domains, which have high permittivity and lower P_r. Thus, the mechanical state likely causes changes in the domain population of the PZT films. These effects of applied strain are also
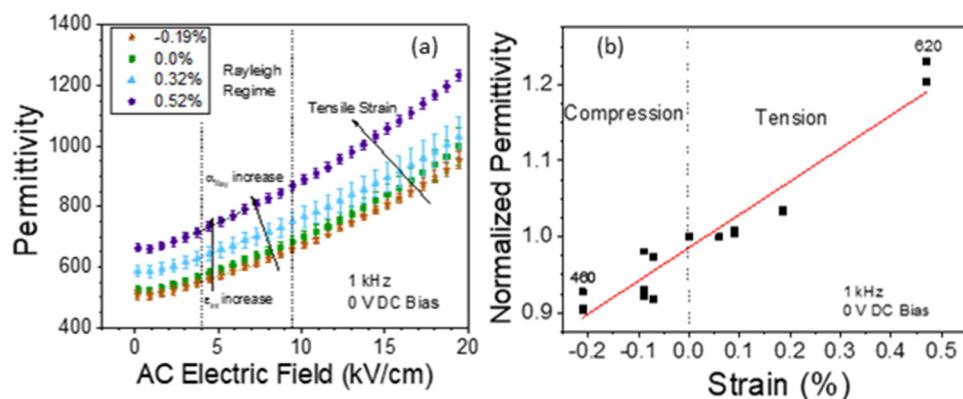
FIG. 4. Permittivity as a function of strain and AC field for the PZT on Ni foil (a) and the normalized permittivity as a function of strain at 5 kV/cm AC field (b). Both ε_{init} and α_{Ray} increased as a function of tensile strain. These low field measurements were at 0 V DC bias.

seen on the effective transverse piezoelectric coefficient ($e_{31,f}$). A lower P_r indicates that fewer domains are aligned parallel to the electric field direction after the field has been removed; the remanent piezoelectric response scales with P_r. Measurements at zero applied strain yielded an $e_{31,f}$ of -9.7 ± 0.45 C/m^2 for films on Ni foil and -7 ± 0.35 C/m^2 for the films on Si. The difference in these values at zero applied strain is related to the different residual stress states and domain populations of the films. Figure 5 shows the changes of $e_{31,f}$ normalized to the zero applied strain value, as a function of applied compressive strain for films on Si. As the compressive stress increased, the magnitude of $e_{31,f}$ increased. The magnitude of this increase depends on whether the film was only poled before or again after the applied static loading to the new strain level allowing for alignment of more c domains.

DISCUSSION

The difference in the P_r and permittivity between the postprocessed two sets of samples corresponds with the residual thermal stresses in the films.[16,22,43] While the PZT composition is close to the morphotropic phase boundary and likely consists of both tetragonal and rhombohedral phases, only the tetragonal domain configurations are considered here, due to the larger difference in P_r and permittivity between in-plane and out-of-plane domains.

Samples on Ni foil were found to have a larger volume fraction of domains with out-of-plane polarization, referred to as the tetragonal c domains, which have a lower permittivity and a higher P_r than in-plane domains or a domains. As a result, PZT films on Ni foil have a lower permittivity and higher P_r. The samples on Si tend to have a lower P_r and higher permittivity because the tensile stress results in a smaller volume fraction of c domains.[16,22,43,44]

As seen in Figs. 3 and 4, an increase in the applied "compressive" stress also increases the P_r and decreases the permittivity, while applied "tensile" stress decreases the P_r and increases the permittivity. These changes suggest the possibility of ferroelastic domain reorientation, as shown in the schematic in Fig. 6. Ideally, the majority of the non-180° domain walls could move, and all domains could undergo ferroelastic switching as suggested in row 2 of Fig. 6. However, the permittivity and P_r on the Ni foil under the highest applied tension did not overlap any of the values of films on Si. This suggests that many of these domains cannot reorient. It is possible that the local strains induced from one domain switching may prevent others from switching as shown in row 3 of Fig. 6.[20] Thus, the reorientation of domains induced by applied tensile stresses at room temperature is insufficient for the films on Ni foils to reach a similar domain state as the samples on Si before mechanical failure ensues. Also, the approximately linear change of both electrical properties as a function of applied strain on Ni foils
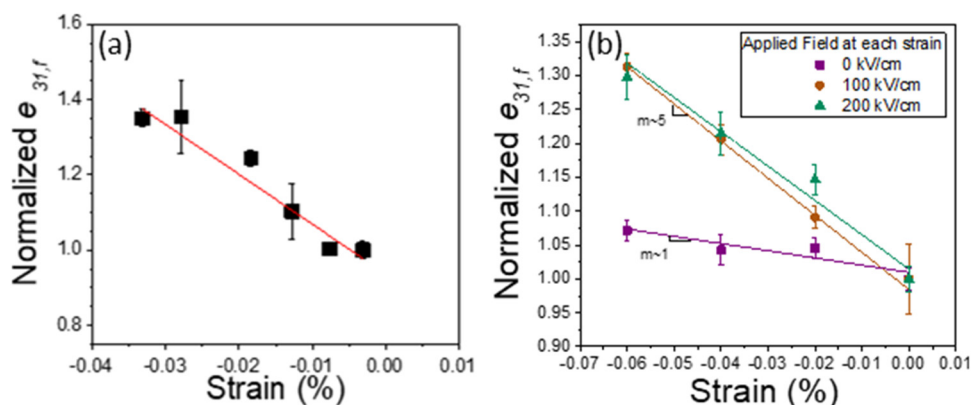

FIG. 5. (a) Normalized $e_{31,f}$ as a function of applied strain for PZT on Si. The magnitude of the $e_{31,f}$ increases under compression linearly. (b) Normalized $e_{31,f}$ with various applied DC biases as a function of compressive strain. m indicates the slope of the linear fit of the normalized $e_{31,f}$ as a function of strain (%); the stain dependence was larger when samples were repoled while under strain.
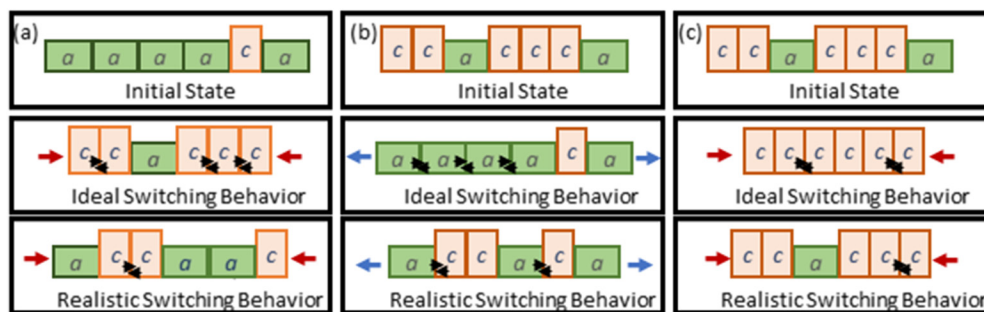
FIG. 6. Schematic of the domain state for (a) the films on Si substrates and (b) and (c) Ni foil. Also shown is how an applied compressive stress could affect the domain state on (a) Si and (c) Ni, as well as how tensile stress might change the domain state for the samples on Ni (b).[20] Red arrows facing inward (→ ←) represent compression. Blue arrows facing outward (← →) represent tension. Black triangles (▶◀) in between domains represent local stresses induced from non-180° domain switching.

indicates that domain reorientation as a function of applied strain may be approximately constant over the strain ranges tested. The linear trend may indicate a wide distribution in the energy potential required for ferroelastic switching. This has been indicated by previous studies[20] but is shown here to persist over much wider strain ranges and a larger total stress magnitude.

In addition, the magnitude of the piezoelectric coefficient increased linearly with applied compressive stress. This also suggests some ferroelastic reorientation of domains.[13] However, the reorientation of ferroelastic domains by stress allows for two ferroelastically equivalent (180°) polarization direction possibilities. That is, when a domains switch to c domains under compression, it is likely that some of these domains will have antiparallel polarization directions (up and down), and thus their charge contributions will cancel out. Therefore, the net piezoelectric response may not be significantly enhanced. However, a DC electric field bias would help align the majority of these reoriented c domains with the field direction, causing them to contribute to the net piezoelectric response and thus produce a significant increase in the piezoelectric coefficient.

The linear trends in the permittivity, remanent polarization, and piezoelectric coefficient are the result of the total stress state of the PZT films. Thus, the applied stresses were added to the residual stresses to provide an estimate of the total stress state for the films on different substrates. As shown in Fig. 7, and supported by Figs. 3(Ic) and 3(IIc), the slope of the normalized P_r is steeper for the films on Si than the films on Ni. As suggested by Wang et al., the films on Si have residual stress states closer to zero stress, which in turn is likely to result in a more complex domain structure, with more non-180° domain walls.[45] This is also supported by estimations from phenomenological values of polarization and permittivity that suggest PZT on Si has roughly 60% c domains, resulting in a mixture of a and c.[42] Assuming a random distribution of domains, this would suggest a high concentration of non-180° domain walls. For PZT on Ni, the phenomenological values of permittivity and polarization suggest predominantly c domains (~70% – 85%), and so these samples would have fewer non-180° domain walls present.[42] Although the Si substrate cannot sustain wider applied strain ranges, the motion of non-180° domain walls affects the

electrical properties more significantly since a and c domains have different properties. This may result in a larger change in the electrical properties for the film on Si for the same applied stress. Conversely, PZT on Ni has a high percentage of c domains and, therefore, a limited number of domains that would be able to ferroelastically switch with applied strains. This may also contribute to the smaller stress dependence of the permittivity. In addition, Fig. 7 emphasizes that while the properties of PZT can be tuned by applied stresses, due to the mechanical limits imposed by failure, the PZT properties on one substrate does not overlap with the properties of the film on the other substrate. As a result, the initial stress state of a film after fabrication largely determines the achievable range of electrical properties.
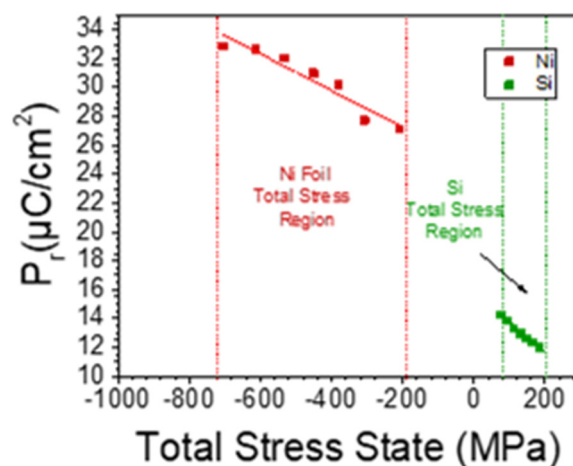
FIG. 7. Working total stress ranges for the films on the two substrates. The difference of these working ranges slightly affects the slope of the properties changes as a function of stress, as well as the complexity of the domain structure in these films on different substrates. Data for this plot come from the experiments shown in Fig. 4.

CONCLUSIONS

The permittivity, remanent polarization, and the piezoelectric properties all depend approximately linearly on the stresses in the PZT film. It was shown that the magnitude of the $e_{31,f}$ of PZT can be improved by applying a DC bias under compressive in-plane stress. Ferroelastic domain switching is possible on PZT films; however, significant improvements in piezoelectric coefficients require alignment of these ferroelasticity switched domains. Although larger strain could be achieved on Ni, the values for permittivity and remanent polarization did not reach those of PZT on Si, indicating the importance of the thermal residual stress in the film on the domain structure.

SUPPLEMENTARY MATERIAL

See the supplementary material for the complete calculation of the residual stress of PZT on both Ni and Si substrates, as well as additional experimental information, and XRD information.

REFERENCES

[1]P. Muralt, R. G. Polcawich, and S. Trolier-McKinstry, MRS Bull. **34**, 658 (2009).
[2]N. Izyumskaya, Y. I. Alivov, S. J. Cho, H. Morkoç, H. Lee, and Y. S. Kang, Crit. Rev. Solid State Mater. Sci. **32**, 111 (2007).
[3]D. Damjanovic, Rep. Prog. Phys. **61**, 1267 (1998).
[4]J. F. Shepard, P. J. Moses, and S. Trolier-McKinstry, Sens. Actuators A Phys. **71**, 133 (1998).
[5]F. Xu, F. Chu, and S. Trolier-McKinstry, J. Appl. Phys. **86**, 588 (1999).
[6]M. Eatough, D. Dimos, B. A. Tuttle, W. L. Warren, and R. Ramesh, MRS Proc. **361**, 111 (1995).
[7]J. F. Shepard, S. Trolier-McKinstry, M. A. Hendrickson, and R. Zeto, in *ISAF '96. Proceedings of the Tenth IEEE International Symposium on Applications of Ferroelectrics, East Brunswick, NJ, 18–21 August 1996* (IEEE, 1996), Vol. 1, p. 161.
[8]M. A. Dubois and P. Muralt, Sens. Actuators A Phys. **77**, 106 (1999).
[9]H. G. Yeo, X. Ma, C. Rahn, and S. Trolier-McKinstry, Adv. Funct. Mater. **26**, 5940 (2016).
[10]S. Trolier-McKinstry, S. Zhang, A. J. Bell, and X. Tan, Annu. Rev. Mater. Res. **48**, 191 (2018).
[11]N. W. Emanetoglu, S. Muthukumar, P. Wu, R. H. Wittstruck, Y. Chen, and Y. Lu, IEEE Trans. Ultrason. Ferroelectr. Freq. Control **50**, 537 (2003).
[12]M. Akiyama, T. Kamohara, K. Kano, A. Teshigahara, Y. Takeuchi, and N. Kawahara, Adv. Mater. **21**, 593 (2009).
[13]J. Ouyang, R. Ramesh, and A. L. Roytburd, Appl. Phys. Lett. **86**, 152901 (2005).
[14]C. B. Yeager, Y. Ehara, N. Oshima, H. Funakubo, and S. Trolier-McKinstry, J. Appl. Phys. **116**, 104907 (2014).
[15]T. Oikawa, M. Aratani, H. Funakubo, K. Saito, and M. Mizuhira, J. Appl. Phys. **95**, 3111 (2004).
[16]B. A. Tuttle, J. A. Voigt, T. J. Garino, D. C. Goodnow, R. W. Schwartz, D. L. Lamppa, T. J. Headley, and M. O. Eatough, in *ISAF '92: Proceedings of the Eighth IEEE International Symposium on Applications of Ferroelectrics, Greenville, SC, 30 August–2 September 1992* (IEEE, 1992), p. 344.
[17]T. A. Berfield, R. J. Ong, D. A. Payne, and N. R. Sottos, J. Appl. Phys. **101**, 024102 (2007).
[18]M. D. Nguyen, M. Dekkers, E. Houwman, R. Steenwelle, X. Wan, A. Roelofs, T. Schmitz-Kempen, and G. Rijnders, Appl. Phys. Lett. **99**, 252904 (2011).
[19]B. A. Tuttle and R. W. Schwartz, MRS Bull. **21**, 49 (1996).
[20]R. J. Zednik, A. Varatharajan, M. Oliver, N. Valanoor, and P. C. McIntyre, Adv. Funct. Mater. **21**, 3104 (2011).
[21]S. B. Desu, J. Electrochem. Soc. **140**, 2981 (1993).
[22]H. G. Yeo and S. Trolier-McKinstry, J. Appl. Phys. **116**, 014105 (2014).
[23]S. C. Lin and W. J. Wu, J. Micromech. Microeng. **23**, 125028 (2013).
[24]H. Hoshyarmanesh, N. Nehzat, M. Salehi, and M. Ghodsi, J. Mech. Sci. Technol. **29**, 715 (2015).
[25]C. Brinker and G. Scherer, *Sol-Gel Science: The Physics and Chemistry of Sol-Gel Processing* (Academic Press, Inc., San Diego, CA, 1990).
[26]D. Das, L. Sanchez, J. Martin, B. Power, S. Isaacson, R. G. Polcawich, and I. Chasiotis, Appl. Phys. Lett. **109**, 131905 (2016).
[27]G. C. A. M. Janssen, M. M. Abdalla, F. van Keulen, B. R. Pujada, and B. van Venrooy, Thin Solid Films **517**, 1858 (2009).
[28]R. J. Ong, D. A. Payne, and N. R. Sottos, J. Am. Ceram. Soc. **88**, 2839 (2005).
[29]E. Chason and P. R. Guduru, J. Appl. Phys. **119**, 191101 (2016).
[30]K. Nishida, M. Osada, S. Wada, S. Okamoto, R. Ueno, H. Funakubo, and T. Katoda, Integr. Ferroelectr. **78**, 281 (2006).
[31]G. A. C. M. Spierings, G. J. M. Dormans, W. G. J. Moors, M. J. E. Ulenaers, and P. K. Larsen, J. Appl. Phys. **78**, 1926 (1995).
[32]J. F. Ihlefeld, D. T. Harris, R. Keech, J. L. Jones, J. P. Maria, and S. Trolier-McKinstry, J. Am. Ceram. Soc. **99**, 2537 (2016).
[33]L. M. Garten and S. Trolier-McKinstry, Appl. Phys. Lett. **105**, 132905 (2014).
[34]M. J. Haun, E. Furman, S. J. Jang, and L. E. Cross, Ferroelectrics **99**, 63 (1989).
[35]D. Damjanovic and M. Demartin, J. Phys. D Appl. Phys. **29**, 2057 (1996).
[36]N. Bassiri-Gharb, I. Fujii, E. Hong, S. Trolier-Mckinstry, D. V. Taylor, and D. Damjanovic, J. Electroceramics **19**, 47 (2007).
[37]H. Nagata, S. W. Ko, E. Hong, C. A. Randall, S. Trolier-McKinstry, P. Pinceloup, D. Skamser, M. Randall, and A. Tajuddin, J. Am. Ceram. Soc. **89**, 2816 (2006).
[38]T. Tani and D. A. Payne, J. Amer. Ceram. Soc. **77**, 1242 (1992).
[39]Y. Okada and Y. Tokumaru, J. Appl. Phys. **56**, 314 (1984).
[40]L. Jordan and W. H. Swanger, Bur. Stand. J. Res. **5**, 1291 (1930).
[41]W. R. Cook, D. A. Berlincourt, and F. J. Scholz, J. Appl. Phys. **34**, 1392 (1963).
[42]M. J. Haun, Z. Zhuang, E. Furman, S. J. Jang, and L. E. Cross, Ferroelectrics **99**, 45 (1989).
[43]C. B. Yeager and S. Trolier-McKinstry, J. Appl. Phys. **112**, 074107 (2012).
[44]W. L. Warren, D. Dimos, B. A. Tuttle, G. E. Pike, M. V. Raymond, R. D. Nasby, R. Ramesh, and J. T. Evans, MRS Proc. **361**, 51 (1995).
[45]J. J. Wang, Y. Wang, J. F. Ihlefeld, P. E. Hopkins, and L. Q. Chen, Acta Mater. **111**, 220 (2016).